Journal of Power Sources 185 (2008) 1471–1477

Contents lists available at ScienceDirect

Journal of Power Sources

journal homepage: www.elsevier.com/locate/jpowsour

Hot corrosion resistance of a Pb–Sb alloy for lead acid battery grids

Wislei R. Osório [a], Claudia S.C. Aoki [b], Amauri Garcia [a,*]

[a] Department of Materials Engineering, University of Campinas – UNICAMP, PO Box 6122, 13083-970 Campinas, SP, Brazil
[b] Research and Development Centre – CPqD Foundation, Rod. Campinas/Mogi, km 118.5, 13086-912 Campinas, SP, Brazil

ARTICLE INFO

Article history:
Received 14 July 2008
Received in revised form 19 August 2008
Accepted 20 August 2008
Available online 26 August 2008

Keywords:
Pb–Sb alloys
Battery grids
Solidification microstructure
Hot corrosion

ABSTRACT

The aim of this study was to evaluate the effects of the microstructural morphologies of a Pb–6.6 wt%Sb alloy on the resulting corrosion resistance in a 0.5 M H_2SO_4 solution at different temperatures: environment temperature, 50 °C and 70 °C. A water-cooled unidirectional solidification system was employed permitting a wide range of microstructures to be analyzed. Electrochemical impedance spectroscopy (EIS) diagrams, potentiodynamic polarization curves and an equivalent circuit analysis were used to evaluate the corrosion behavior of the Pb–Sb alloy samples. It was found that with increasing temperatures the general corrosion resistance of Pb–Sb dendritic alloys decreases, and that independently of the working temperature finer dendritic spacings exhibit better corrosion resistance than coarser ones.

1. Introduction

It is well known that the solution characteristics, such as pH and temperature may affect the corrosion mechanism and the corrosion behavior of metallic alloys [1–3]. Lead acid batteries manufacturers have introduced modifications in the grid project in order to permit both the battery grid weight and the production costs to be reduced, as well as to increase the battery life-time cycle and the corrosion resistance [4–6]. The performance of lead acid batteries in automotive applications can also be significantly affected by temperature variations.

The improvement on the corrosion resistance of as-cast metallic alloys is strongly dependent on the microstructural arrangement, which in turn depends on the cooling rate imposed during solidification, which affects both the scale of the cellular and dendritic patterns and the solute redistribution, and on the electrochemical behavior of solute and solvent [7–16]. Recent studies have shown that as-cast Pb–Sb alloys with finer dendritic microstructures tend to yield higher corrosion resistances at room temperature than coarser dendritic arrangements. In contrast, when such alloys have a cellular microstructure an opposite behavior occurs with higher corrosion resistances being connected with coarser cellular microstructures [11,12].

Generally, the growth of regular cells is favored by low growth rates during solidification and/or low solute content. On the other hand, dendritic arm spacings are typical of alloys with higher solute content and/or solidified under higher growth rates. A recent study has characterized cellular and dendritic microstructural patterns as a function of casting thermal parameters for Pb–Sb hypoeutectic alloys [17].

The manufacturers have indicated a working temperature range for batteries from about −10 °C to 70 °C. Such high temperature can be easily attained in severe automotive operation. In order to evaluate and compare the corrosion resistance of dendritic morphologies of a Pb–6.6 wt%Sb alloy as a function of temperature (environment temperature, 50 °C and 70 °C) corrosion tests were carried out in a 0.5 M H_2SO_4 solution. Techniques such as electrochemical impedance spectroscopy (EIS), potentiodynamic polarization curves and an equivalent circuit method were used to provide results for the comparative analysis.

2. Experimental procedure

The Pb–6.6 wt%Sb alloys were prepared from commercially pure metals: Pb (99.97 wt%) and Sb (99.86 wt%).

A water-cooled unidirectional solidification system was used to provide a wide range of dendritic microstructures (from coarse to fine). More details concerning this solidification set-up can be obtained from previous articles [11,12,17]. The cylindrical ingot was sectioned on a midplane, ground, polished and etched with a solution to reveal the macrostructure. Transverse sections (perpendicular to the growth direction) along the ingot length were polished and etched with a solution (37.5 cm^3 of glacial acetic acid and 15 cm^3 of H_2O_2, at 25 °C) for microscopy examination. Image

* Corresponding author. Tel.: +55 19 3521 3320; fax: +55 19 3289 3722.
E-mail address: amaurig@fem.unicamp.br (A. Garcia).

0378-7753/$ – see front matter © 2008 Elsevier B.V. All rights reserved.
doi:10.1016/j.jpowsour.2008.08.040

processing systems Neophot 32 (Carl Zeiss, Esslingen, Germany) and Leica Quantimet 500 MC (Leica Imaging Systems Ltd., Cambridge, England) were used to measure the dendritic spacing.

In order to evaluate the corrosion behavior of the Pb–Sb alloy samples collected at different positions along the casting length, corrosion tests were performed in a 1 cm^2 circular area of ground (600 grit SiC finish) sample surfaces. A 0.5 M H_2SO_4 solution at 25 °C, 50 °C and 70 °C, a calomel electrode reference and a platinum counter electrode were used to perform the corrosion tests. The working temperatures of 50 °C and 70 °C were chosen in order to evaluate the electrochemical behavior of the battery grid material in more severe working temperature conditions.

EIS measurements began after an initial delay of 30 min for the sample to reach a steady-state condition. A potentiostat coupled to a frequency analyzer system, a glass corrosion cell kit with a platinum counter electrode and a saturated calomel reference electrode (SCE) were used. The working electrodes consisted of casting alloy samples which were positioned at the glass corrosion cell kit, leaving a circular 1 cm^2 metal surface in contact with the electrolyte. The potential amplitude was set to 10 mV in open-circuit potential and the frequency range was set from 100 mHz to 100 kHz. The samples were further ground to a 600 grit SiC finish, followed by distilled water washing and air drying before measurements.

Polarization tests were also carried out in a 500 cm^3 of sulfuric acid solution (500 mol × m^{-3} or 0.5 M) at 25 °C using an EG & G Princeton Applied Research, model 273A potentiostat at the same positions where the afore-mentioned EIS tests were carried out. A scan rate of 0.2 mV s^{-1} from −250 mV (SCE) to +250 mV (SCE) related to open-circuit potential was used. This mentioned potentiodynamic range is corresponding to −1200 mV and −700 mV vs. Hg/Hg_2SO_4 electrode (MSE). The EIS experimental results were analyzed by equivalent circuits which were proposed by using the ZView® software.

3. Results and discussion

The three positions along the casting length from where the samples for corrosion tests were collected are shown in Fig. 1(a). Secondary dendritic arm spacings (λ_2) are also shown in Fig. 1(a) corresponding to each position from the casting/chill surface (from the bottom to the casting top). The experimental cooling rate dependences on secondary dendrite arm spacing are shown in Fig. 1(b). It can be seen that the use of a water-cooled mold imposes higher cooling rates close to the casting bottom and a decreasing profile along the casting length due to the increase of the thermal resistance of the solidified shell with distance from the cooled surface.

The typical microstructures observed along the cross sections of the Pb–6.6 wt%Sb alloy casting are shown in Fig. 2. The microstructure immediately after solidification consists of a completely dendritic array, constituted by a Pb-rich matrix (α-phase: solid solution of Sb in Pb) with a eutectic mixture in the interdendritic regions formed by α, and a Sb-rich β-phase (solid solution of Pb in Sb).

The experimental EIS diagrams at 25 °C, 50 °C and 70 °C in a 0.5 M H_2SO_4 solution are shown in Fig. 3. In previous articles [7–16,18,19], it has been shown that both the modulus of impedance (Z) and the phase angle (θ) decrease with increasing distance from the casting bottom for dendritic alloys (casting/chill interface). As a direct consequence, both impedance and phase values decrease with increasing secondary dendrite arm spacings (λ_2). It is well known that higher impedance and phase angle are conducive to a nobler electrochemical behavior. Thus, a finer dendritic microstructure provides better corrosion resistance than a coarser one. This tendency has also been verified for samples in a 0.5 M H_2SO_4 solution

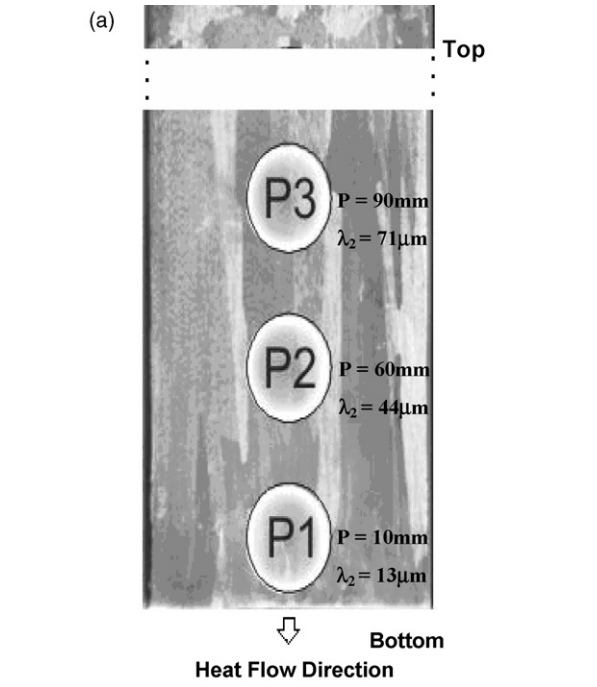

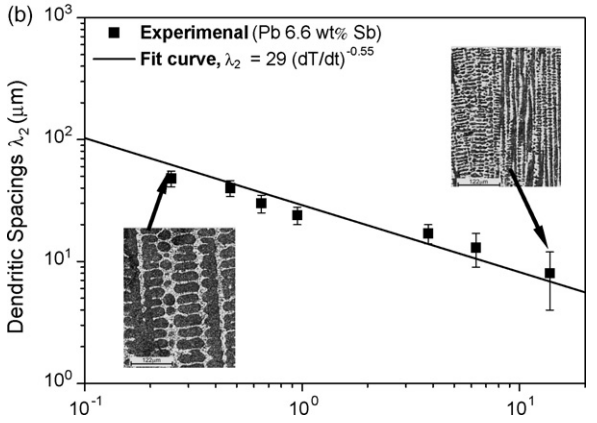

Fig. 1. (a) Typical macrostructure of a Pb–6.6 wt%Sb alloy casting: P is the position from the casting bottom where samples were collected for the corrosion tests and λ_2 is the measured secondary dendrite arm spacing; (b) λ_2 as a function of cooling rate (the line represents an empirical fit to the experimental points).

at 50 °C. On the other hand, both the Z and θ decrease if compared to the results of the test performed at 25 °C. The parameters Z and θ for samples tested at 50 °C decreased of about three times and 20%, respectively, when compared to those of tests carried out at 25 °C. At 70 °C, Z and θ decreased about 12 times and 70%, respectively, if compared to the corresponding values which resulted from tests at 25 °C. However, the electrochemical behaviors were very similar for the three samples experimentally examined and no correlation with the dendritic pattern could be established. It is not surprising that the corrosion resistance decreases at elevated temperatures. As expected, the experimental results of EIS have shown that both working temperatures, 50 °C and 70 °C, provoke a considerable decrease on the corrosion resistance, when compared to the values obtained for correspondent positions at 25 °C.

Fig. 4 shows the potentiodynamic polarization curves that have confirmed the occurrence observed in the EIS diagrams. It seems that the dendritic arrangement controls the corrosion evolution. In this context, a finer dendritic microstructure can provide better corrosion resistance than a coarser one. For the tests carried out at

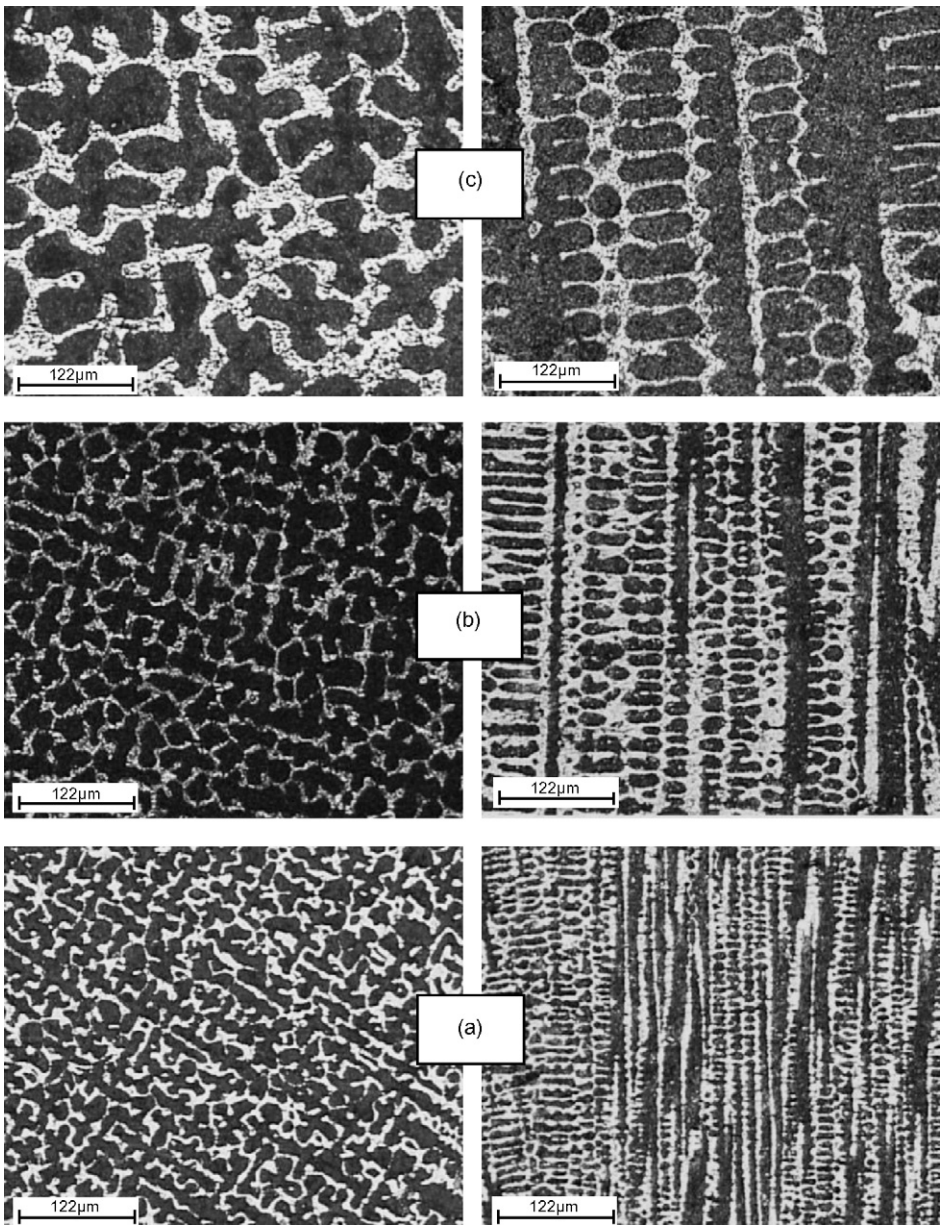

Fig. 2. (a) Typical optical microstructure of a Pb–6.6 wt%Sb alloy at transversal and longitudinal sections evidencing the dendritic pattern. Secondary dendrite arm spacing: (a) λ_2 = 08 μm (P = 5 mm); (b) λ_2 = 15 μm (P = 20 mm) and (c) λ_2 = 42 μm (P = 50 mm).

50 °C and 70 °C, the three samples collected along the casting length (P1, P2 and P3, as shown in Fig. 1(a)) have presented similar I_{Corr} of about 70 μA cm^{-2} and 90 μA cm^{-2}, respectively, as shown in Fig. 4. At 25 °C, I_{Corr} has varied from 25 μA cm^{-2} to 35 μA cm^{-2}, for fine (bottom) and coarse (top) dendritic microstructures, respectively [12].

Passive current densities (I_{PP}) have been observed for the three samples collected along the castings for both tests carried out at 25 °C and 50 °C. It can be observed that I_{PP} increases with increasing working temperatures. At both 25 °C and 50 °C, the I_{PP} for P1 indicates that a more defective anodic layer consisted by Pb and Sb ions, $PbSO_4$, oxygen and OH^- particles has grown at the surface. This suggests that P1 with a finer dendrite arrangement has been less corroded compared to the other two positions. At 25 °C, the I_{PP} for P1 and the two other positions (P2 and P3) are of about 5.5×10^{-5} and 2.75×10^{-5} A cm^{-2}, respectively. At 50 °C, the I_{PP} for P1 and the two other positions are of about 12×10^{-5} and 7×10^{-5} A cm^{-2}.

At 70 °C, above −450 mV, only P2 and P3 tend to have anodic layer formation. This is clear evidence that even at higher working temperatures the dendritic pattern has a strong influence on the corrosion behavior.

It is important to remark that the corrosion behavior analysis of the present work differs from studies of PbO/PbO_2 formation which consider the corrosion of the lead electrode and proceed at much higher potentials [20,21]. It is evident that higher temperatures can significantly affect the charge/discharge mechanism of lead acid batteries. However, the present work focuses on the role of the dendritic array of Pb–Sb alloys battery grids on its electrochemical behavior.

It is known that the open-circuit potential of a pure lead electrode in 0.5 M H_2SO_4 solution is −950 mV vs. Hg/Hg_2SO_4 (MSE). Although the SCE electrode is not commonly used in lead acid system studies, a SCE electrode can also be used as a reference electrode since the one inconvenient (the fact that chloride may

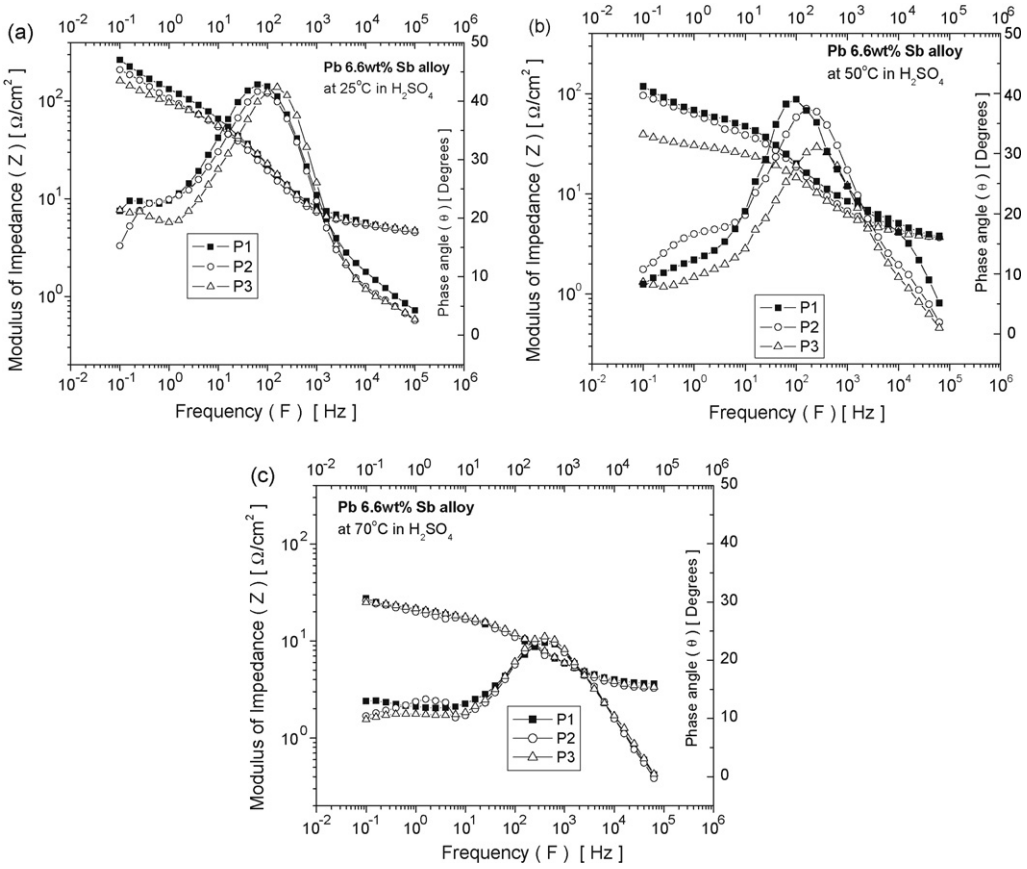

Fig. 3. Experimental EIS diagrams for the Pb–6.6 wt%Sb alloy as a function of secondary dendritic spacing (P1, P2, P3 as shown in Fig. 1(a)) for tests carried out at (a) 25 °C; (b) 50 °C and (c) 70 °C.

contaminate the electrolyte), and other is to convert from SCE to MSE or other potential scales (ASTM G3). The open-circuit potential of Pb–Sb alloys is something lower than pure lead (−950 mV vs. MSE) due to the accelerated self-discharge related to lower hydrogen over voltage on Sb [20–22].

Concerning the processes taking place on the working electrode surface, it is important to remark that the solubility of $PbSO_4$ in 0.5 M H_2SO_4 is relatively high, and only small amounts of $PbSO_4$ crystals will be formed and reduced (dissolution–precipitation mechanism). At potentials above −950 mV (MSE) anodic oxidation of Pb takes place and Pb(II) ions are formed. Some $PbSO_4$ crystals are formed on the electrode surface which, after long enough polarization will form a semi-permeable membrane which, on turn, will passivate the electrode surface. Due to the low potential values neither PbO nor PbO_2 will be formed in the potential ranges selected in this study. Indeed, both Sb(III) and Sb(V) ions will be also not formed. PbO can be formed in the potential above −450 mV (MSE) and PbO_2 above +950 mV (MSE) [20–22]. In the potential range selected Pb^{2+} will be formed or reduced along with some hydrogen evolution. A $PbSO_4$ membrane layer will be formed on the electrode surface (passivation) but not any PbO (stronger passivation), antimony ions or mixed Pb–Sb oxides [20–22]. It is known that the rate of anodic oxidation of Pb to Pb(II) ions at potentials about −0.8 V is not the process that determines the corrosion rate of lead in sulfuric acid. In addition to the anodic oxidation of lead, at potentials above −0.40 V another anodic process begins in which Sb oxidation to Sb(III) and Sb(V) is involved. These processes are systematically detailed by Pavlov et al. [20–22].

In order to supply quantitative support for the discussions of these experimental EIS results, an appropriate model (ZView®) for equivalent circuit quantification has also been used. Mainly the properties of the double layer will be revealed and will allow drawing conclusions about the nature and rate of the oxidation processes.

Fig. 5 depicts the proposed equivalent circuit and Fig. 6 shows the experimental data and the examples of experimental and simulated agreement for positions P1 and P3, in Nyquist diagrams for the three temperatures experimentally examined. The equivalent circuit is similar to one proposed in the literature and used in previous studies [7–16,18,19,23–25]. The electronic equivalent circuit consists of a capacitance component ($Z_{CPE(1)}$) in parallel to series resistors, R_1 and R_2, and another capacitance component ($Z_{CPE(2)}$) in parallel to R_2. In this model, R_{el} corresponds to the resistance of the electrolyte (0.5 M H_2SO_4 solution) which in Bode diagram is expressed in a high frequency limit ($F > 1$ Hz). R_1 and R_2 are the resistances of the oxide layer [23–25] which are associated to the charge transfer resistance through the vacancies of the porous layer and the participation of adsorbed intermediates. $Z_{CPE(1)}$ corresponds to the capacitance of the porous layer and $Z_{CPE(2)}$ to the capacitance of the barrier layer which seems to correspond to the double layer formation. A constant-phase element representing a shift from an ideal capacitor was used instead of the capacitance itself, for simplicity. The impedance of a phase element is defined as $Z_{CPE} = [C(j\omega)^n]^{-1}$, where C is the capacitance, ω is the frequency and $-1 \leq n \leq 1$. The value of n seems to be associated with the non-uniform distribution of current as a result of roughness and surface defects [14–16,23–25]. The impedance parameters are shown in Fig. 6 and Table 1. The fitting quality was evaluated by chi-squared (χ^2) values, which were interpreted by the ZView® software.

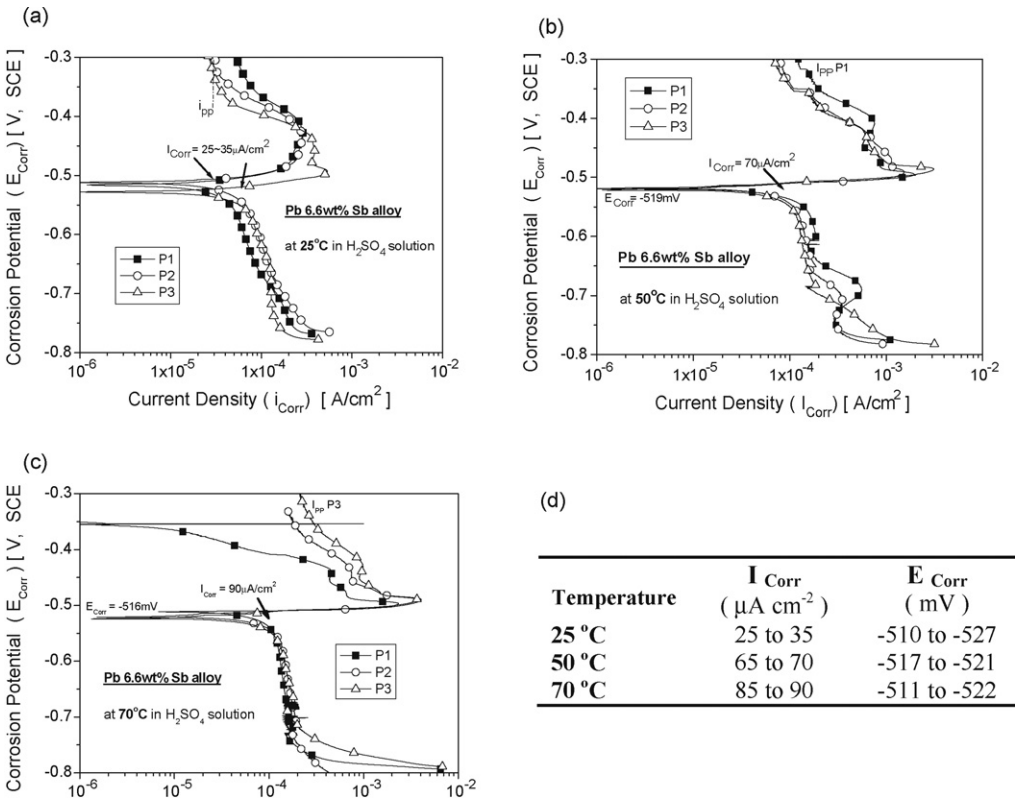

Temperature	I_{Corr} (μA cm^{-2})	E_{Corr} (mV)
25 °C	25 to 35	-510 to -527
50 °C	65 to 70	-517 to -521
70 °C	85 to 90	-511 to -522

Fig. 4. Experimental potentiodynamic polarization curves for the Pb–6.6 wt%Sb alloy as a function of dendritic spacing (P1, P2, P3 as shown in Fig. 1(a)) at: (a) 25 °C; (b) 50 °C; (c) 70 °C, respectively; and (d) corresponding corrosion current density (I_{Corr}) and corrosion potential (E_{Corr}) values.

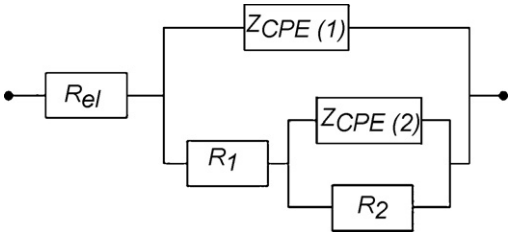

Fig. 5. Proposed equivalent circuit by using the ZView® software.

Nyquist plots reveal that the diameters of the inductive arcs at P1 are higher than those at P3 for all temperatures examined. These results are similar to those analyzed in Bode and Bode-phase diagrams and polarization curves.

A comparative analysis between the impedance parameters for the tests carried out at 25 °C, 50 °C and 70 °C is presented in Fig. 7. It can be observed that the capacitances ($Z_{CPE(1)}$) and the polarization resistances (R_1) decrease with distance from the casting bottom (from P1 to P3). However, it can be seen that the capacitances increase with increasing working temperatures. At 70 °C, R_1 is significantly higher due to the corrosion products formation in this severe working temperature. This has been confirmed by the polarization curves and by the experimental EIS diagrams shown in Fig. 4.

Although the capacitances ($Z_{CPE(2)}$) which are associated with the barrier layer are similar at P1, P2 and P3 for any temperature examined, these values also increase with increasing working temperatures (as $Z_{CPE(1)}$). Associated to this, the polarization resistances (R_2) of the barrier layer decrease, which is an indication that the corrosion resistance decreases with increasing temperature (Fig. 6).

Although there exist other impedance parameters, as shown in Table 1, for samples at position P1 (at 25 °C, 50 °C and 70 °C), analyses of the capacitances and the resistances obtained by the equivalent circuit technique, the EIS results and the potentiodynamic polarization curves indicate that coarser dendritic microstructures (at position P3) are more susceptible to the corrosion action independently of the working temperature.

It is known that the dendritic microstructure of a Pb–Sb alloy is mainly formed by α-phase (less noble) and by an interdendritic region which has a lamellar eutectic morphology (mixture of α

Table 1
Impedance parameters for the Pb–6.6 wt%Sb alloy at position P1 in a 0.5 M H_2SO_4 solution

Parameters	P1 (20°C)	P1 (50°C)	P1 (70°C)
R_{el} (Ω cm^{-2})	4.83	3.71	3.54
$Z_{CPE(1)}$ (μF cm^{-2})	854.03 (±12.4)	896.01(±88.9)	1265 (±132)
$Z_{CPE(2)}$ (mF cm^{-2})	5.89 (±0.4)	16.20 (±0.15)	79.32 (±7.4)
n_1	0.63	0.60	0.63
n_2	0.85	0.30	0.37
R_1 (Ω cm^{-2})	160	108	7×10^8
R_2 (Ω cm^{-2})	190	52	14
χ^2	20×10^{-4}	9.2×10^{-3}	2.0×10^{-3}

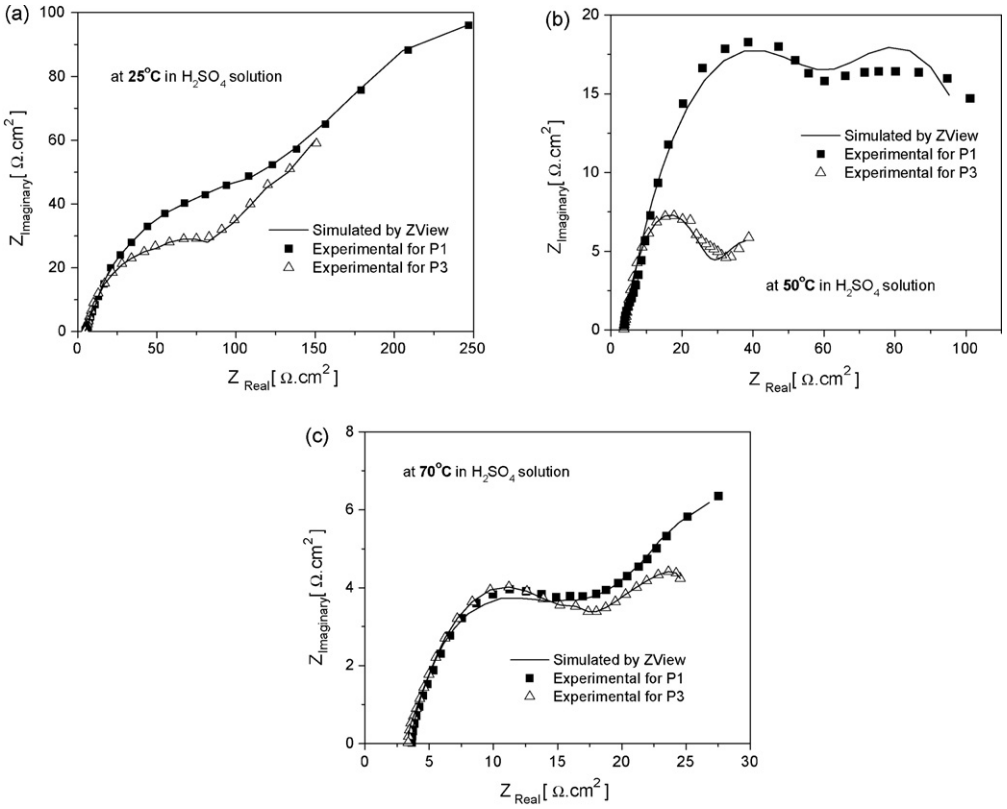

Fig. 6. Nyquist diagrams with experimental results and curves simulated by the ZView® software: (a) at 20 °C; (b) at 50 °C and (c) 70 °C (for positions P1 and P3 as shown in Fig. 1(a)).

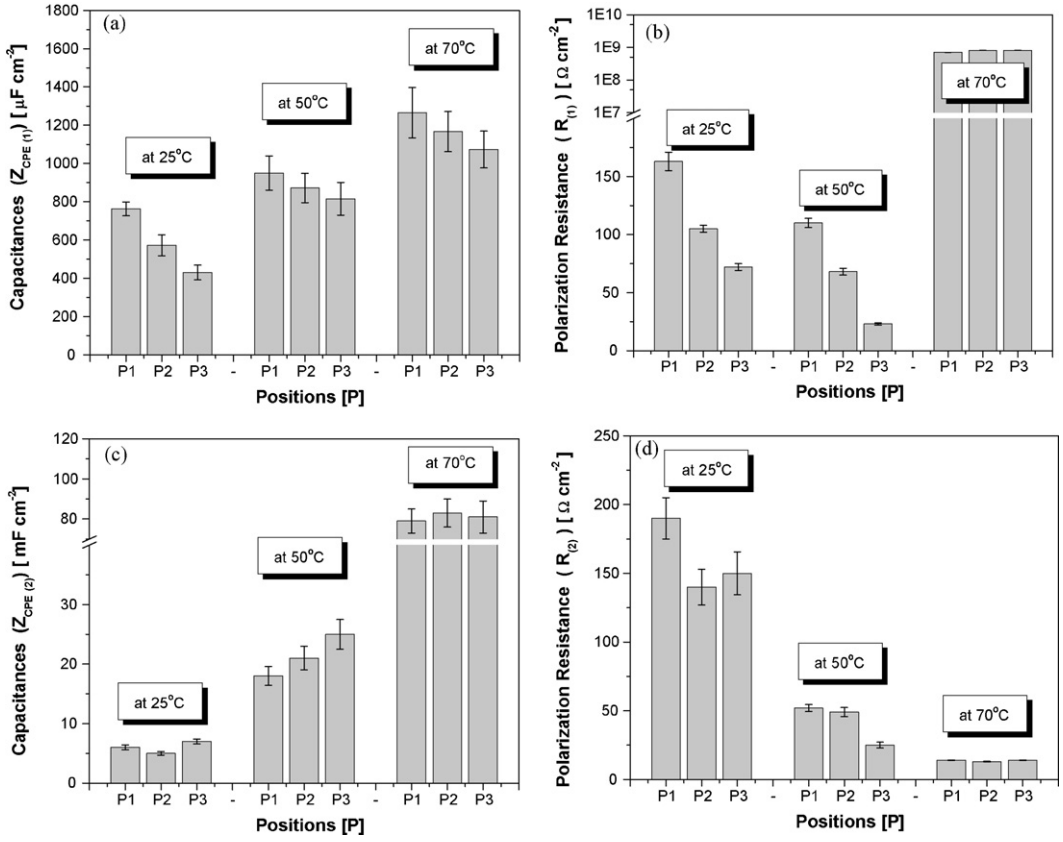

Fig. 7. Capacitances and polarization resistances obtained by using the ZView® software: (a) $Z_{CPE(1)}$; (b) R_1; (c) $Z_{CPE(2)}$ and (d) R_2 for positions P1, P2 and P3, as shown in Fig. 1(a).

and β phases), as shown in Fig. 2. A more extensive distribution of the Pb-rich dendritic matrix (less noble regions), which is associated to smaller dendritic spacings, will have the eutectic mixture which contains the nobler β (Sb-rich) phase "enveloping" the Pb-rich regions and thus providing a better corrosion resistance. On the other hand, a coarser dendritic structure will have the larger Pb-rich regions more exposed and thus favoring the corrosion action.

It is important to remark that the high working temperatures modify the kinetics of the corrosion products formation (such as $PbSO_4$) and considerably decrease the corrosion resistance of the battery grids manufactured with dendritic Pb–Sb alloys. The high working temperatures can also significantly affect the charge/discharge mechanism of lead acid batteries, and consequently decrease the battery life-time.

4. Conclusions

The present experimental investigation permits the following conclusions to be drawn:

- The experimental EIS diagrams, potentiodynamic polarization curves and fitted equivalent circuit parameters have shown that finer dendritic arrays tend to yield higher corrosion resistances than coarser dendritic structures for a hypoeutectic Pb–6.6 %wtSb alloy. The dendritic array morphology has the antimony-rich regions located in the lamellar eutectic mixture. The Sb-rich lamellae will envelope the Pb-rich phase more efficiently for finer dendritic spacings due to the more extensive distribution of the eutectic mixture, and thus protecting the Pb-rich matrix.
- Analyses of the experimental results provided by EIS tests and potentiodynamic polarization curves in a 0.5 M H_2SO_4 solution at 25 °C, 50 °C and 70 °C and the results furnished by the proposed equivalent circuit permit to conclude that high working temperatures modify significantly the electrochemical behavior of a Pb–6.6 wt%Sb alloy casting. Despite the experimental evidence of properties of the double layer and about the nature and rate of the oxidation processes at the surface of the samples, it seems that the dendritic arrangement controls the corrosion evolution. However, high temperatures provide an accelerated corrosion products formation decreasing the corrosion resistance.
- Independent of the working temperature, casting samples with finer dendritic microstructures have better corrosion resistance than coarser ones. It is known that a fine dendritic array is provided by high cooling rates during solidification. Thus, a high cooling rate casting process would be more appropriate for the manufacturing of battery grids with Pb–Sb dendritic alloys (>3 wt%Sb) due to the expected higher corrosion resistance.

Acknowledgements

The authors acknowledge financial support provided by FAPESP (The Scientific Research Foundation of the State of São Paulo, Brazil), FAEPEX– UNICAMP, CNPq (The Brazilian Research Council) and and CPqD (Research and Development Centre, Campinas, Brazil).

References

[1] S. Magaino, M. Soga, K. Sobue, A. Kawaguchi, N. Ishida, H. Imai, Electrochim. Acta 44 (1999) 4307–4312.
[2] A.V. Benedetti, P.L. Cabot, J.A. Garrido, A.H. Moreira, Electrochim. Acta 45 (2000) 2187–2195.
[3] W.R. Osório, C.M.A. Freire, A. Garcia, Rev. Metal. Madrid Extra (2005) 160–164.
[4] R.D. Prengaman, J. Power Sources 95 (2001) 224–233.
[5] R.D. Prengaman, in: K.R. Bullock, D. Pavlov (Eds.), Advances in Lead-Acid Batteries, 84-14, The Electrochemical Society, Pennington, NJ, 1984, p. 201.
[6] B. Rezaei, S. Damiri, J. Solid State Electrochem. 9 (2005) 590–594.
[7] W.R. Osório, C.M.A. Freire, A. Garcia, Mater. Sci. Eng. A 402 (2005) 22–32.
[8] W.R. Osório, C.M.A. Freire, A. Garcia, J. Alloys Compd. 397 (2005) 179–191.
[9] W.R. Osório, C.M.A. Freire, A. Garcia, J. Mater. Sci. 40 (17) (2005) 4493–4499.
[10] W.R. Osório, P.R. Goulart, G.A. Santos, C. Moura Neto, A. Garcia, Metall. Mater. Trans. 37A (2006) 2525–2537.
[11] D.M. Rosa, J.E. Spinelli, W.R. Osório, A. Garcia, J. Power Sources 162 (2006) 696–705.
[12] W.R. Osório, D.M. Rosa, A. Garcia, J. Power Sources 175 (2008) 595–603.
[13] W.R. Osório, P.R. Goulart, A. Garcia, Mater. Lett. 62 (2008) 365–369.
[14] W.R. Osório, N. Cheung, J.E. Spinelli, P.R. Goulart, A. Garcia, J. Solid State Electrochem. 11 (2007) 1421–1429.
[15] D.Q. Martins, W.R. Osório, M.E.P. Souza, R. Caram, A. Garcia, Electrochim. Acta 53 (2008) 2809–2817.
[16] A. Cremasco, W.R. Osório, C.M. Freire, A. Garcia, R. Caram, Electrochim. Acta 53 (2008) 4867–4875.
[17] D.M. Rosa, J.E. Spinelli, A. Garcia, J. Alloys Compd. 422 (2006) 227–238.
[18] M. Kliskic, J. Radosevic, S. Gudic, M. Smith, Electrochim. Acta 43 (1998) 3241–3255.
[19] S. Gudic, J. Radosevic, M. Kliskic, Electrochim. Acta 47 (2002) 3009–3016.
[20] D. Pavlov, M. Bojinov, T. Laitinen, G. Sundholm, Electrochim. Acta 36 (1991) 2087–2092.
[21] D. Pavlov, M. Bojinov, T. Laitinen, G. Sundholm, Electrochim. Acta 36 (1991) 2081–2086.
[22] D. Pavlov, B. Monahov, G. Sundholm, T. Laitinen, J. Electroanal. Chem. 305 (1991) 57–63.
[23] J. Pan, D. Thierry, C. Leygraf, Electrochim. Acta 41 (1996) 1143–1153.
[24] M. Aziz-Kerrzo, K.G. Conroy, A.M. Fenelon, S.T. Farell, C.B. Breslin, Biomaterials 22 (2001) 1531–1538.
[25] S.L. Assis, S. Wolynec, I. Costa, Electrochim. Acta 51 (2006) 1815–1819.